Anal. Chem. **2003,** *75,* 4766−4772

Room-Temperature Single-Nucleotide Polymorphism and Multiallele DNA Detection Using Fluorescent Nanocrystals and Microarrays

Daniele Gerion,*[,†,‡,§] Fanqing Chen,*[,∥] Balaji Kannan,[⊥] Aihua Fu,[†] Wolfgang J. Parak,[†,‡] David J. Chen,[∥] Arunava Majumdar,[‡,⊥] and A. Paul Alivisatos[†,‡]

Department of Chemistry and Department of Mechanical Engineering, University of California, Berkeley, California 94720, and Materials Sciences Division and Life Sciences Division, Lawrence Berkeley National Laboratory, Berkeley, California 94720

We report two cDNA microarray-based applications of DNA−nanocrystal conjugates, single-nucleotide polymorphism (SNP) and multiallele detections, using a commercial scanner and two sets of nanocrystals with orthogonal emissions. We focus on SNP mutation detection in the human p53 tumor suppressor gene, which has been found to be mutated in more than 50% of the known human cancers. DNA−nanocrystal conjugates are able to detect both SNP and single-base deletion at room temperature within minutes, with true-to-false signal ratios above 10. We also demonstrate microarray-based multiallele detection, using hybridization of multicolor nanocrystals conjugated to two sequences specific for the hepatitis B and hepatitis C virus, two common viral pathogens that inflict more than 10% of the population in the developing countries worldwide. The simultaneous detection of multiple genetic markers with microarrays and DNA−nanocrystal conjugates has no precedent and suggests the possibility of detecting an even greater number of bacterial or viral pathogens simultaneously.

Genotyping of human diseases and detection of pathological microorganisms, such as infectious virus and biowarfare reagents, depend mainly on the molecular detection of nucleic acids or proteins. The advent of microarray and microanalytical device analysis has provided unprecedented high throughput, convenience, capability, and opportunities for genotyping and microorganism detection.[1,2] Many detection assays are performed with reaction volumes in the microliter or nanoliter range. Detection of biological samples at such extremely low amounts is a major challenge for clinical diagnosis and detection. Most biochemical assays require secondary detection of a label, because biomolecules lack intrinsic properties that are useful for direct high-sensitivity detection. Most assays are based on hybridization or specific interaction, which exploit the high binding specificity of nucleic acids and polypeptides. Label detection is a key determinant of sensitivity. The continuing quest for improved labels has produced a series of markers, including new fluorophores such as cyanine dyes, enzymes, and particles such as phosphors and nanocrystals[3,4] (for further reviews, see also ref 5).

Among the most commonly used labels in biological diagnostics are organic fluorescent dyes. But while new types of fluorescent microscopes and techniques have pushed the resolution well below the diffraction limit of light,[6] fluorescent probes have not followed the same impressive evolution trend. Organic dyes still suffer from notorious limitations such as photobleaching and discrete excitation bands that preclude their use in many applications. An alternative technology, based on inorganic semiconductor nanocrystals, might overcome some of these limitations. These materials are crystals made of semiconductor CdSe/ZnS core/shell structures and have a diameter of a few nanometers.[7] Nanocrystals possess many properties that make them attractive for biolabeling: broad excitation spectrum but narrow and precise tunable emission[6] by simply varying the size of the nanoparticles (see Figure 1), negligible photobleaching,[8] fairly high quantum yields, stability, and negligible phototoxicity.[9] Recent synthetic progress has allowed the conjugation of nanocrystals to a wide variety of biomolecules such as DNA,[10−12] proteins,[13,14] antibod-

* To whom correspondence should be sent. E-mails: gerion1@llnl.gov (D.G.); f_chen@lbl.gov (F.C.).

† Department of Chemistry, University of California.

‡ Materials Sciences Division, Lawrence Berkeley National Laboratory.

§ Present address: Lawrence Livermore National Laboratory, P.O. Box 808, L-415, Livermore, CA 94551.

∥ Life Sciences Division, Lawrence Berkeley National Laboratory.

⊥ Department of Mechanical Engineering, University of California.

(1) van Ingen, C. *Nat. Genet.* **2002**, *32*, 463−463.

(2) Brown, P. O.; Botstein, D. *Nat. Genet.* **1999**, *21*, 33−37.

(3) Taton, T. A.; Mirkin, C. A.; Letsinger, R. L. *Science* **2000**, *289*, 1757−1760.

(4) Park, S. J.; Taton, T. A.; Mirkin, C. A. *Science* **2002**, *295*, 1503−1506.

(5) Kricka, L. J. *Ann. Clin. Biochem.* **2002**, *39*, 114−129.

(6) Lacoste, T. D.; Michalet, X.; Pinaud, F.; Chemla, D. S.; Alivisatos, A. P.; Weiss, S. *Proc. Natl. Acad. Sci. U.S.A.* **2000**, *97*, 9461−9466.

(7) Dabbousi, B. O.; RodriguezViejo, J.; Mikulec, F. V.; Heine, J. R.; Mattoussi, H.; Ober, R.; Jensen, K. F.; Bawendi, M. G. *J. Phys. Chem. B* **1997**, *101*, 9463−9475.

(8) Gerion, D.; Pinaud, F.; Williams, S. C.; Parak, W. J.; Zanchet, D.; Weiss, S.; Alivisatos, A. P. *J. Phys. Chem. B* **2001**, *105*, 8861−8871.

(9) Parak, W. J.; Boudreau, R.; Le Gros, M.; Gerion, D.; Zanchet, D.; Micheel, C. M.; Williams, S. C.; Alivisatos, A. P.; Larabell, C. *Adv. Mater.* **2002**, *14*, 882−885.

(10) Parak, W. J.; Gerion, D.; Zanchet, D.; Woerz, A. S.; Pellegrino, T.; Micheel, C.; Williams, S. C.; Seitz, M.; Bruehl, R. E.; Bryant, Z.; Bustamante, C.; Bertozzi, C. R.; Alivisatos, A. P. *Chem. Mater.* **2002**, *14*, 2113−2119.

(11) Pathak, S.; Choi, S. K.; Arnheim, N.; Thompson, M. E. *J. Am. Chem. Soc.* **2001**, *123*, 4103−4104.

(12) Dubertret, B.; Skourides, P.; Norris, D. J.; Noireaux, V.; Brivanlou, A. H.; Libchaber, A. *Science* **2002**, *298*, 1759−1762.

10.1021/ac034482j CCC: $25.00
Published on Web 08/20/2003

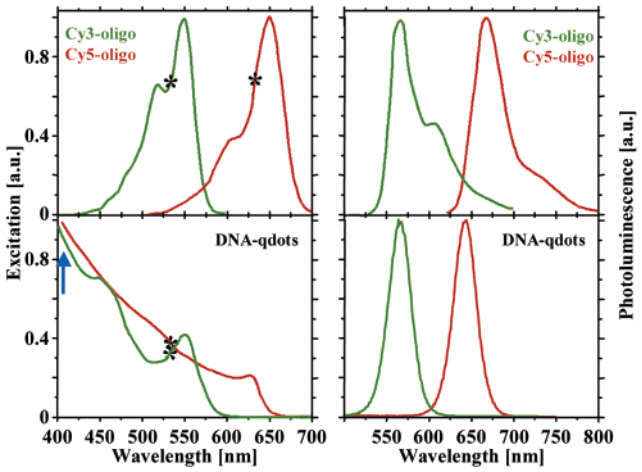

Figure 1. Comparison of the excitation and fluorescence of Cy3−oligos, Cy5−oligos (19-mer), and yellow and red DNA−nanocrystals (not to scale). Note that yellow and red nanocrystals are the same material but differ only in the size of the nanocrystal core. The dyes spectra are adapted from the Amersham Bioscience website. The asterisks in the excitation spectra indicate the wavelengths of excitation used in this study (532 and 634 nm). Emission of Cy3−oligos and Cy5−oligos are 566 and 668 nm, respectively. Yellow C5−nanocrystals (566 nm, fwhm ~32 nm) and red B3−nanocrystals (644 nm, fwhm ~34 nm) are used in this study. Excitation at 408 nm with a blue laser diode (blue arrow) is a better choice to excite nanocrystals.

ies,[15,16] short peptides,[17] or neurotransmitters[18] and their targeting to their receptor sites. Until now though, biological applications of these biomodified nanocrystals are still in their infancy because of the delicate process of synthesizing and manipulating them. Ongoing improvements however have already led to in vivo targeting, and there is great hope of using nanocrystal technology in more complex biological problems.

One of these applications is DNA microarrays. Advances in this technology have allowed high-throughput gene expression profiling and nucleotide polymorphism detection, which have profound implications in medical sciences. Indeed, small variations in the genome influence our predisposition to diseases, such as cancer, and congenital genetic diseases.[19−21] The identification of these variations has become a major issue in genetics since they are believed to be major determinants to disease onset, progression, and clinical prognosis. Also, such small variations are extremely useful in categorization of infectious disease pathogens, such as the highly mutable HIV,[22] and the classification of biowarfare reagents, such as anthrax.[23,24] These variations include insertions, deletions, rearrangements of the sequences, or alterations of a single base pair also called single-nucleotide polymorphism (SNP). Although DNA microarray technology using conventional organic fluorescent dyes is extremely powerful in detecting multiple genetic markers with high throughput, it presents a certain number of drawbacks, such as high incubation temperature requiring special ovens, overnight incubation time, and possible leakage of a peculiar fluorescent color in another channel caused by overlapping spectra.[25] Each of these shortcomings limits the potential of DNA microarrays.

In recent years, DNA−nanocrystal conjugates have emerged as efficient probes, capable of hybridizing to the complement strands and generating up to five perfectly orthogonal channels of detection within the visible range.[6] Combined with their high sensitivity, DNA−nanocrystal probes are ideal candidates for DNA microarrays with an even higher throughput. So far however, DNA−nanocrystal probes have been tested only in proof-of-concept experiments where they were exposed to either their fully complement sequence or a fully random one as a control.[11,12,26] The possibility to pinpoint some genetic variations in the genome remained purely theoretical.

We report, in this article, the first study of DNA−nanocrystal conjugates as efficient probes in SNP human genotyping and pathogen detection using cDNA arrays. Specifically, we focus on mutation detection in human oncogene p53, a tumor suppressor gene, which has been found to be mutated in 50% of the known cancers.[27−29] Our model experiments have used a SNP located at amino acid residue 248, on exon 7 of p53, which is one of the most common mutation hot spots in p53.[30] In addition, we also demonstrate the feasibility of simultaneous detection of multiple biological pathogens, by using hepatitis B virus (HBV) and hepatitis C virus (HCV) as a widespread model system. The anti-HCV and anti-HBV positive rate in the general population or healthy blood donors is 2−10% worldwide.[31,32] With our detection system based on nanocrystal-conjugated probe DNA and microarray, we have been successful in identifying multiplexed HBV and HCV targets. The potential single-molecule detection sensitivity of nanocrystals could enable the direct detection of large numbers (hundreds or thousands) of pathogens at the same time on a microarray, thus serving as a replacement technology for PCR.

In all our experiments, hybridization of DNA−nanocrystal probes is extremely fast (~10 min) and is performed at room temperature. Signal-to-background ratios of >100 can be readily

(13) Goldman, E. R.; Balighian, E. D.; Mattoussi, H.; Kuno, M. K.; Mauro, J. M.; Tran, P. T.; Anderson, G. P. *J. Am. Chem. Soc.* **2002**, *124*, 6378−6382.
(14) Chan, W. C. W.; Nie, S. M. *Science* **1998**, *281*, 2016−2018.
(15) Wu, X. Y.; Liu, H. J.; Liu, J. Q.; Haley, K. N.; Treadway, J. A.; Larson, J. P.; Ge, N. F.; Peale, F.; Bruchez, M. P. *Nat. Biotechnol.* **2003**, *21*, 41−46.
(16) Jaiswal, J. K.; Mattoussi, H.; Mauro, J. M.; Simon, S. M. *Nat. Biotechnol.* **2003**, *21*, 47−51.
(17) Akerman, M. E.; Chan, W. C. W.; Laakkonen, P.; Bhatia, S. N.; Ruoslahti, E. *Proc. Natl. Acad. Sci. U.S.A.* **2002**, *99*, 12617−12621.
(18) Rosenthal, S. J.; Tomlinson, A.; Adkins, E. M.; Schroeter, S.; Adams, S.; Swafford, L.; McBride, J.; Wang, Y. Q.; DeFelice, L. J.; Blakely, R. D. *J. Am. Chem. Soc.* **2002**, *124*, 4586−4594.
(19) Knudson, A. G. *Am. J. Med. Genet.* **2002**, *111*, 96−102.
(20) Altshuler, D.; Kruglyak, L.; Lander, E. *N. Engl. J. Med.* **1998**, *338*, 1626.
(21) Kruglyak, L. *Nat. Genet.* **1999**, *22*, 139−144.
(22) Ball, J. K.; Holmes, E. C.; Whitwell, H.; Desselberger, U. *J. Gen. Virol.* **1994**, *75* (Pt. 4), 67−79.
(23) Keim, P.; Kalif, A.; Schupp, J.; Hill, K.; Travis, S. E.; Richmond, K.; Adair, D. M.; Hugh-Jones, M.; Kuske, C. R.; Jackson, P. *J. Bacteriol.* **1997**, *179*, 818−824.
(24) Read, T. D.; Salzberg, S. L.; Pop, M.; Shumway, M.; Umayam, L.; Jiang, L.; Holtzapple, E.; Busch, J. D.; Smith, K. L.; Schupp, J. M.; Solomon, D.; Keim, P.; Fraser, C. M. *Science* **2002**, *296*, 2028−2033.
(25) Schena, M.; Shalon, D.; Davis, R. W.; Brown, P. O. *Science* **1995**, *270*, 467−470.
(26) Gerion, D.; Parak, W. J.; Williams, S. C.; Zanchet, D.; Micheel, C. M.; Alivisatos, A. P. *J. Am. Chem. Soc.* **2002**, *124*, 7070−7074.
(27) Hollstein, M.; Sidransky, D.; Vogelstein, B.; Harris, C. C. *Science* **1991**, *253*, 49−53.
(28) Denissenko, M. F.; Pao, A.; Tang, M.; Pfeifer, G. P. *Science* **1996**, *274*, 430−432.
(29) Denissenko, M. F.; Chen, J. X.; Tang, M. S.; Pfeifer, G. P. *Proc. Natl. Acad. Sci. U.S.A.* **1997**, *94*, 3893−3898.
(30) Pfeifer, G. P. *Mutat. Res.* **2000**, *450*, 155−166.
(31) Hwang, S. J. *J. Microbiol. Immunol. Infect.* **2001**, *34*, 227−234.
(32) Geller, S. A. *Clin. Liver Dis.* **2002**, *6*, 317−334, v.

obtained in conditions that discriminate down to three base mismatches in a 25-mer sequence. No false positive signals are observed when formamide is used in the hybridization solution. We also pinpoint more stringent conditions for hybridization that lead to SNP detection with true-to-false signal ratios over 10. All this is achieved with a commercial scanner that is not optimized for nanocrystal detection. Overall, our results might be a first step toward the use of nanocrystal probes for an ultrafast detection of a great number of viral or bacterial pathogens simultaneously.

EXPERIMENTAL SECTION

Array Layout. Two sets of arrays are produced for this study.

Set 1. 10 rows of 6 identical spots each row.

Row 1. cDp53a: 5′-aggatgggcctcAggttcatgccgc-3′.

Row 2. cDp53c: 5′-aggatgggcctcCggttcatgccgc-3′.

Row 3. cDp53g: 5′-aggatgggcctcGggttcatgccgc-3′.

Row 4. cDp53t: 5′-aggatgggcctcTggttcatgccgc-3′.

Row 5. cDp53x: 5′-aggatgggcctc-ggttcatgccgc-3′.

Row 6. Dp53g, which is the reverse complement of cDp53c with a G in the middle place: 5′gcggcatgaaccGgaggcccatcct-3′.

Row 7. cB3 is the reverse complement to portion of the HBV genomic sequence (hepatitis B virus sequence, Genebank accession number AF461043):5′-cgagattgagatcttctgcgacgcggcgattgagaccttcgtctgcgaggcgagggagttcttcttctag-3′.

Row 8. cC5 is the reverse complement to portion of the HCV genomic sequence (hepatitis C virus sequence, Genebank accession number D90208): 5′-ctagacgctttctgcgtgaagacagtagttcctcacaggggagtgatctatggtggagtgtcgcccccaa-3′.

Row 9. B3, which is the reverse complement of cB3: 5′-ctagaagaagaactccctcgcctcgcagacgaaggtctcaatcgccgcgtcgcagaagatctcaatctcg-3′.

Row 10. C5, which is the reverse complement of cC5: 5′-ttgggggcga cactccacca tagatcactc ccctgtgagg aactactgtc ttcacgcaga aagcgtctag ccatggcgtt-3′.

Set 2. DNA with mismatches for SNP detection. 10 rows, 3 spots for each DNA, 2 types of DNA per row.

Row 1. cDp53t and 5bpm@end.

Row 2. 10 bpm@end and 15 bpm@end.

Row 3. 20bpm@end and 3bpm@center.

Row 4. 7bpm@center and 11bpm@center.

Row 5. 15 bpm@center and blank.

Row 6. cDp53a and cDp53c.

Row 7. cDp53g and cDp53t.

Row 8. cDp53x and Dp53t.

Row 9. cC5 (HCV capture probe) and cB3 (HBV capture probe).

Row 10. C5 and B3.

Sequences from 5′ to 3′ end.

cDp53a: aggatgggcctcaggttcatgcgcgc.

5bpm@end: aggatgggcctcaggttcatATATA.

10bpm@end: aggatgggcctcaggCATCCATATA.

15bpm@end: aggatgggccCACATCATCCATATA.

20bpm@end: aggatAATACCACATCATCCATATA.

3bpm@center: aggatgggcctATAgttcatgcgcgc.

7bpm@center: aggatgggccAATACCAcatgcgcgc.

11bpm@center: aggatgggCTAATACCAACtgcgcgc.

15bpm@center: aggatgCACTAATACCAACCAcgcgc.

Oligonucleotide Synthesis. The following sequences were custom-synthesized at Operon. The wild-type 25-mer encompassing the amino acid residue 248 on exon 7 of the human p53 oncogene is called cDp53a. The nucleotide in the middle of the cDp53a sequence is mutated into either A, C, G, or T or deleted to generate oligonucleotides cDp53a, cDp53c, cDp53g, cDp53t, and cDp53x. The 5′s of the above sequences are modified with a C-12 amino linker (Glen Research). cDp53t (5′-gcggcatgaaccT-gaggcccatcct-3′) sequence, which is from the wild-type p53 and complements to Dp53a sequences, is conjugated to nanocrystals.

We also synthesized four sequences corresponding to genomic sequences in hepatitis virus B and hepatitis virus C. (1) cB3 is reverse complement to a portion of the HBV genomic sequence (hepatitis B virus sequence, Genebank accession number AF461043). cB3 will capture HBV genomic DNA. (2) cC5 is reverse complement to a portion of the HCV genomic sequence (hepatitis C virus sequence, Genebank accession number D90208). cC5 will capture the HCV genomic DNA. (3) B3, which is a reverse complement of cB3, is conjugated to nanocrystals and can be specifically captured by cB3 on the microarray. (4) C5, which is a reverse complement of cC5 is conjugated to the nanocrystals and can be specifically captured by cC5 on the microarray. The four hepatitis B/C virus related sequences are also amino-modified at the 5′ end of the oligonucleotides.

Fabrication of Microarray. The amino-modified cDp53a,c,g,t,x, Dp53t, and other sequences were diluted to 25 μM in a 1:1 mixture of 3× SSC buffer and microprinting buffer from Telechem. The printing of the microarray has been carried out by a state-of-art high-speed microarrayer OmniGrid II from GeneMachine, with SMP3 Stealth split pins from Telechem. Pin speed is 2 cm/s, and dwell time on slide is 25 ms. Humidity is maintained at 45%. Sonication and washing are carried out between samples to avoid sample carryover. Glass slides with an aldehyde-activated surface (Superaldehyde slide from Telechem) were used for the microprinting of the microarrays. After printing, the DNA with amino end modification is allowed to react to the aldehyde group overnight to form a covalent link between the DNA probe and the microarray substrate surface before being subjected to further processing.

Processing of the DNA Array Slide. The arrays are hydrated for ∼15 min in a humid atmosphere. They are washed twice for 2 min in 0.1% Tween 20 in water, twice 1 min in ddH_2O. Then the Schiff base is reduced in (25% methanol in 50 mM phosphate buffer) and 5 g/L sodium borohydride. The slides are washed again twice for 1 min in 0.1% Tween 20 in water and 1-min final wash in ddH_2O. The slides are dried by centrifugation for 1 min at 500*g*. A rubber seal defines eight reaction compartments of ∼40 μL each.

DNA−Nanocrystal Synthesis and Purification. Core/shell CdSe/ZnS nanocrystals, with core size of ∼2.5 (yellow emission) and ∼4 nm (red emission), are embedded in a silica shell, which confers them high stability in high-salt buffers and in a wide ranges of pHs. The polymerized shell can be tailored to have any electric charge and to contain a wide array of functional groups (thiols, amines, carboxyls). The resulting nanoparticles have ∼10 nm in diameter and resemble very much globular proteins. Single-stranded DNA of any length can be covalently linked to nanoparticles by standard bioconjugation techniques. Each nanoparticle is likely to carry a few DNA. The synthesis of these biolabels has been extensively described elsewhere.[8,10] The bioconjugates are

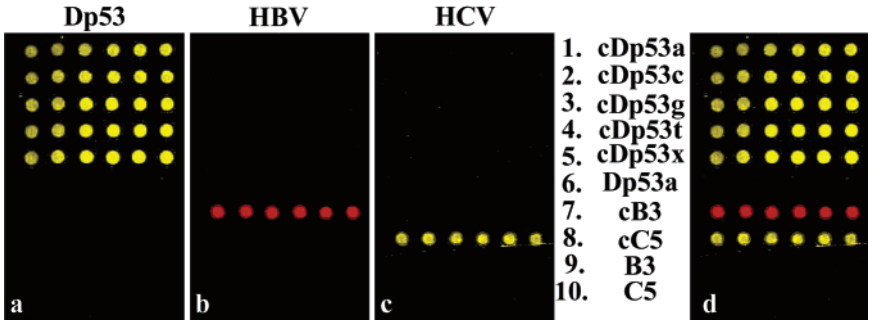

Figure 2. Multicolor targeting of SNP mutations in human oncogene p53 (rows 1−6) and of human hepatitis B and C viruses (rows 7−10) with different DNA−nanocrystal probes. The arrays are printed in 10 rows of 6 identical blots. The five top rows are 25-mers related to the sequence encompassing the amino acid residue 248 on exon 7 of the human oncogene p53 called Dp53. The nucleotide in the middle of the cDp53 is mutated in either A, C, G, T or deleted X and generates cDp53a, cDp53c, cDp53g, cDp53t, or cDp53x, respectively. Row 6 contains Dp53g, the complement sequence of cDp53c. Row 7 is cB3, the reverse complement to a portion of the 3′ end of HBV. Row 8 is cC5, the reverse complement to a portion of the 3′ end of HCV. Row 9 is B3 the complement of the sequence cB3, and row 10 is C5, the complement of the sequence cC5.a) In panel a, yellow Dp53g−nanocrystals are targeted only toward mutations in human oncogene p53, but SNP detection is not achieved. In panel b, red B3−nanocrystals are targeted toward the hepatitis B virus sequence. In panel c, yellow C5−nanocrystals are targeted only toward the hepatitis C virus sequence. Panel d is an overlay of panels a−c. Note that in both red and yellow channels, signal-to-noise ratio is >100, and no cross-talk is observed. Incubation time is ∼1 h. Each spot is ∼100 μm.

purified from excess of free DNA by electrodialysis in 5−10 mM phosphate buffer, pH ∼7.3, in a 200-μL Teflon chamber. The chamber is closed by two regenerated cellulose membrane of 100 000 MWCO. We apply a voltage of 3−5 V/cm, I ∼10−15 mA for a period of 45 min to ensure a complete removal of free DNA. The DNA−nanocrystal conjugates are collected from the dialysis chamber, diluted to 500 μL, and concentrated in a Microcon 100 down to ∼50 μL. This procedure is repeated twice. The concentration of the DNA−nanocrystal solution is checked by UV−visible spectroscopy. We consider extinction coefficients of 3×10^5 mol^{-1} cm^{-1} at 555 nm for yellow- (emission 565 nm) and 9×10^5 mol^{-1} cm^{-1} at 630 nm for red-emitting (emission 644 nm) nanocrystals, respectively. The quantum yields are estimated at ∼20 and 5% for yellow and red samples, respectively. Purified samples are stable for months. However, hybridization efficiency was observed to drop after a few days, a fact attributed to wrapping of the oligo around the particle. We recover the initial hybridization efficiency by applying a small voltage (∼3−5 V/cm) to the DNA−nanocrystal conjugates. This step is performed in the electrodialysis chamber with the same conditions described above.

DNA−Nanocrystal Hybridization and Washing. DNA−nanocrystal conjugates are diluted to the desired concentration for hybridization. All reactions, including the incubation, are performed at room temperature, on a rocking platform. Typically, we use 40 μL of nanocrystal solution in 10 mM potassium phosphate buffer, 30 mM NaCl, 0.1% Tween 20, and 30−70% formamide. Concentrations of nanocrystals vary from a few nanomolar to 1 μM. Incubation time is typically 1 h but can be as low as ∼10 min. The arrays are then washed for 30 s in 10 mM phosphate buffer, 300 mM NaCl followed by 1 min in pure water. The slides are then dried by a brief centrifugation, after which they are ready for imaging.

Imaging and Analysis. Fluorescence from the arrays is measured with a commercial objective-scanning confocal Axon 3000i scanner (Axon Instruments), which has two excitation laser diodes (532 and 635 nm). Two orthogonal detection channels, for yellow and red fluorescence, respectively, are detected with two distinct photomultipliers. Both yellow and red channels are saved as 8-bit jpg images independently. A homemade Matlab routine allows the processing of the images to calculate the histogram of each blots. The average fluorescence intensity for each oligonucleotide printed on the slide is determined and then normalized with respect to the intensity of the spots corresponding to the perfect complement sequence.

RESULTS

Multicolor DNA Array with Mild Hybridization Conditions. The first set of experiments intends to probe the possibility of using DNA−nanocrystal conjugates and microarrays for hepatitis genotyping and detection in the presence of a background of human genes. For this purpose, we choose two particular sequences specific to HBV and HCV and a third sequence specific to human oncogene p53. We call them B3, C5, and Dp53, respectively. B3 and C5 are 75-mers corresponding to portions of the HBV and HCV, respectively. Dp53 is a 25-mer, covering the 25 nucleotides flanking codon 248 in gene p53; its 13th (central) base is a T, and hence, we will call it Dp53t. These three sequences are independently conjugated to the nanocrystals and their complements (cB3, cC5, cDp53a, respectively—cDp53a means the oligonucleotide sequence is complement to Dp53 and that its 13th base is an "A") are printed on the DNA array.

These sequences allow us to monitor the specificity of hybridization and the possibility of recording nonoverlapping (orthogonal) channels using an Axon microarray scanner (Axon Instruments). Previous experiments using gold patterns suggest that 10 mM phosphate buffer, 50 mM NaCl, and 0.1% Tween 20, pH ∼7.3, is a reasonable incubation buffer.[26] Using these conditions, we target yellow Dp53t−nanocrystal conjugates to cDp53a (Figure 2, panel a). In panel b, red B3-nanocrystals are targeted to cB3, while in panel c, yellow C5−nanocrystals are targeted to cC5. Panel d is an overlay of the previous panels.

Due to their relatively narrow emission (Figure 1), yellow nanocrystals are never seen in the red channel and red nanocrystals do not appear in the yellow channel of the Axon scanner. It is therefore clear from Figure 2 that DNA−nanocrystals are targeted to their complement strands without cross-talks. These

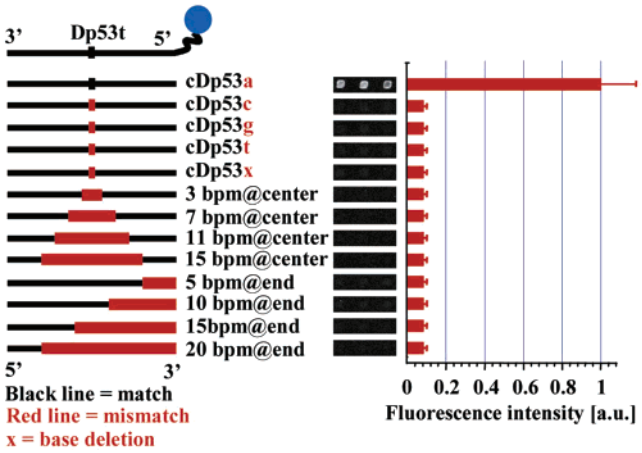

Figure 3. Geometry for probing SNP in human oncogene p53. On the left, the schematic of the 25-mer sequences used to probe SNP detection. From the perfect complement sequence, cDp53a, we introduce more and more base mismatches either at the center or at the 3′ end. The sequences of all oligonucleotides are given in the Experimental Section. On the right side, a composite image of the array after 1 h of hybridization in 70% formamide, 30 mM NaCl, 0.1% Tween 20. The only signal visible comes from the position of the perfect complement, cDp53a. The histogram for each sequence shows that signal-to-background ratio is ∼12. Incubation time is ∼1 h, but we also observe SNP detection for incubation times as short as 10 min. Each spot is ∼100 μm.

perfectly orthogonal channels are detected with signal to surrounding background ratios, also called signal-to-noise ratio, as high as 150. For a given set of hybridization conditions but for different slides, the intensities of the spot signals are constant within 15−20%.

Although C5 and B3 are quite long (75-mers), they do not bear any homologies longer than seven bases with themselves or with cDp53a. On the other hand, cDp53a and its single-base mutants show up with about the same intensity, and therefore, SNP detection is not reached with such mild hybridization conditions. Different washing stringencies, including heat, do not yield to SNP detection either. This first set of experiments tells us that DNA−nanocrystal probes can easily discriminate genotypes with low homologies, such as the three we used here. However, a wider application of these probes in multiplexed genotyping would require the possibility to detect SNP.

Conditions To Reach SNP Selectivity: Effects of Formamide and Salt Concentrations. To precisely pinpoint the conditions for SNP detections, we focus on the sequence specific to human oncogene p53, Dp53t, and its complement cDp53a. We print on the array 13 sequences of 25 bases homologous to cDp53a but with an increasing number of base mismatches either at the center or at the 3′ end. We also print on the array the sequences specific to HBV and HCV as background genes, but we will not consider them hereafter since they never yield any signal. Figure 3 illustrates schematically the structure of the sequences homologous to cDp53a printed on the slide and indicates where the mismatches are located. The right part of Figure 3 also shows that Dp53t−nanocrystal probes achieve SNP detection. The ratio of the signal from the complement spot to the signal from the SNP spots, also called the true-to-false signal ratio, is ∼12. Notice here that all noncomplement sequences give a signal that reaches the noise floor. The key strategy to achieve such selectivity is to use unfavorable conditions for hybridization so that only DNA−nanoparticle conjugates with a perfect match have a chance to hybridize. As a result, although the overall signal is lower, the discrimination between the perfect match sequence and the SNP sequences is higher.

DNA arrays are ideal to explore these unfavorable conditions. Low-salt concentrations only, i.e., 2−10 mM NaCl, do not yield to SNP detection. A combination of low-salt concentrations and the presence of denaturing organic solvents such as formamide are necessary, much like the case of dye-labeled oligos. We thus performed a two-dimensional study varying independently the salt concentration and the formamide content in the hybridization process. We monitored the intensity of the signal of each cDp53a homologues on the array.

Figure 4a summarizes the effect of formamide content while keeping 30 mM NaCl in the incubation buffer. With no formamide, the perfect match sequence (column 1, cDp53a) and the sequences with SNP homologues (columns 2−5) have nearly the same intensity, arbitrarily set to 1 for the perfect match. In this peculiar case, we observe a prominent false-positive signal from column 6, corresponding to a mutant sequence with a three-base mismatch in the center. All other sequences show a negligible contribution. The signal from the three-base mismatch mutant can be reduced by increasing the content of formamide in solution. At 40% formamide in the incubation buffer, the intensity of the three-base mismatch mutant is similar to the intensity of cDp53a, but SNP detection is not yet reached. At 60% formamide, the false-positive signal is totally suppressed and we observe SNP detection with a true-to-false ratio of ∼2. At slightly higher formamide content, we reach the peak of selectivity. Only the perfect match sequence cDp53a gives a signal. All other mutant sequences are totally black. The signal-to-noise ratio as well as the true-to-false ratio is ∼12. A further increase in formamide content to 80% does not produce any hybridization at all.

Similarly, for a fixed amount of formamide in solution (Figure 4b), the hybridization gets less and less selective as the salt concentration is increased. At 70% formamide, 10 mM NaCl, no hybridization occurs, while at 30 mM NaCl we observe the highest selectivity. With increasing concentrations of NaCl, the signal-to-noise ratio gets bigger, but SNP detection becomes weaker. Also, there are no false positive signals in this case. At relatively high salt concentration, i.e., 100 mM NaCl, SNP detection is almost lost. A signal from the three-base mismatch mutant sequence (column 6) appears with intensity ∼3 times lower than that of cDp53a.

Sensitivity of the Probes. The high selectivity of DNA−nanoparticle conjugates constitutes only one step for their use in cDNA microarray technology. A second aspect is related to the sensitivity of the probe. We have performed titration experiments by targeting DNA−nanoparticles to their complement sequence. Figure 5 illustrates the case of yellow B3−nanoparticles targeted to the reverse complement to a portion of the 3′ end of HBV genomic sequence. As indicated in the inset, a positive identification of a printed sequence requires ∼2 nM concentration of DNA−nanoparticle probes. In comparison, we can detect the same sequence using about 10−50 pM Cy5-DNA. This comparison is only indicative here since the sensitivity of nanocrystal probes cannot be fully assessed with our setup because the Axon scanner

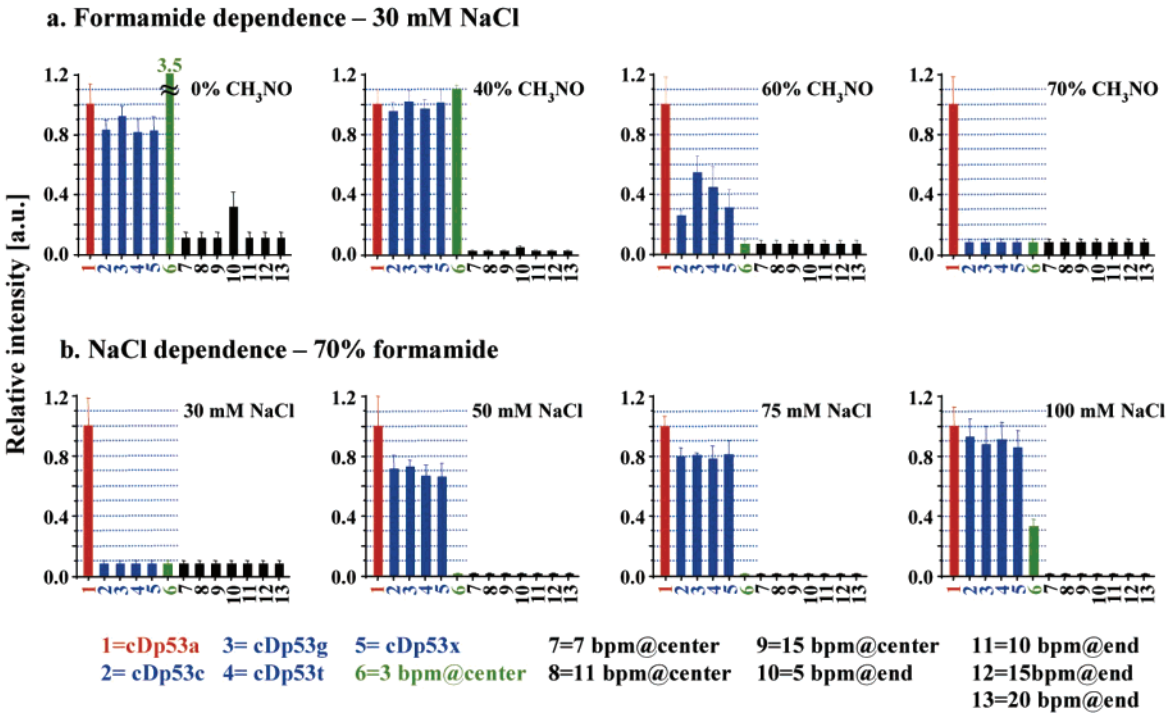

Figure 4. Evolution of SNP detection in human p53 versus hybridization conditions. We report the intensity of the signal on the spots of the DNA sequences of Figure 2 as a function of hybridization conditions. In all these graphs, lane 1 is the perfect match sequence, cDp53a. Its intensity is the reference and is set to 1. Lanes 2−13 correspond to the sequences described in Figure 2 (i.e., 2 = cDp53c, ..., 13 = 20bpm@end). Reducing stringencies, by either increasing the formamide concentration or reducing the NaCl concentration, leads to SNP with a true-to-false signal ratio of ∼12. Note how, with formamide in solution, SNP is progressively lost as [NaCl] is increased. In this case, at 75 mM NaCl, only sequences with a single-base difference give a signal. At 100 mM, the sequence with a three-base mismatch at the center (lane 6) give a signal $\sim^1/_3$ of the complement sequence.

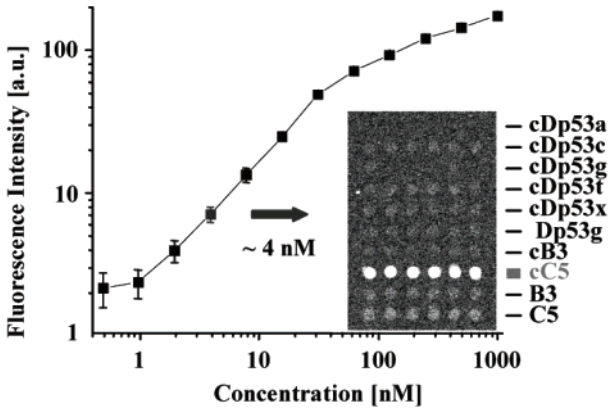

Figure 5. Titration curve for sensitivity determination. Yellow C5−nanocrystals are hybridized at different concentration. The intensity of the signal is measured as a function of the concentration of C5−nanoparticle conjugates. We consider an extinction coefficient of 3 × 10^5 M^{-1} cm^{-1}at 555 nm, the exciton peak of the yellow C5−nanocrystals. Inset: At ∼4 nM, the hybridization signal is still clearly visible with a signal-to-noise ratio of ∼2. Present resolution is ∼2 nM, but the true sensitivity of the nanocrystal technology cannot be fully assessed with our nonoptimized Axon scanner. Incubation time is ∼1 h. Each spot is ∼100 μm.

is only optimized for Cy3 and Cy5 dyes and not for nanocrystal photophysics.

DISCUSSION

Our results show that DNA−nanocrystal probes of different colors are able to target hepatitis B and C genotypes in the presence of a background of human genes, such as p53. Such simultaneous detection of multiple pathogens has never been reported before for microarray-based nanocrystal labeling. We see potential applications in clinical diagnosis with an expanded number of pathogens. With improvements of sensitivity down toward the single-molecule detection level, where nanocrystals are regularly studied, our method could have the potential to be a replacement technology for PCR**.** However, for that to be realized, a number of modifications will have to be implemented as will be discussed further on. Indeed, nanocrystal technology is attractive in many aspects. Even if the sequences specific to HBV and HCV are G−C rich (∼68%), we do not observe significant false-positive artifacts. We believe the same conclusion holds true for any genotype, since G−C base pairing is stronger than A−T and G−C content can reach 25−75% in bacterial genomes but only 41% in the human genome.[33] Therefore, the use of DNA−nanocrystal probes in cDNA microarrays suppresses the issue of cross-talks between detection channels. This constitutes a marked improvement compared to certain sets of organic dyes commonly used, especially for high-sensitivity applications such as gene expression profiling. In all our experiments, we used yellow- and red-emitting nanocrystals with emissions at 566 (fwhm ∼32 nm) and 644 nm (fwhm ∼34 nm), respectively, and no leakage on the opposite channel is ever observed (Figure 1). Moreover, due to their low adsorption on glass, DNA−nanocrystal conjugates yield fairly large signal-to-noise ratios over 100 that are reproducible with different microarray slides.

(33) Lander, E. S.; et al. *Nature* **2001**, *409*, 860−921.

A further interesting aspect is the selectivity of the DNA−nanocrystal conjugates. In fact, cDNA sequences with more than 3 base mismatches with DNA−nanoparticle probes do not produce any signal in an extremely wide range of hybridization conditions. The cDNA homologues that yield a measurable signal are the full complement sequence, its SNP mutants, and the three-base pair mutant. If no formamide is present during the incubation, the three-base pair mutant sometimes gives the largest signal, a signature of false-positive detection. This strong false-positive signal appears in many different slides but its origin is still unclear. A simple speculation may attribute it to the peculiar interaction of the DNA and the nanoparticle favoring locally a non-Watson−Crick base pairing. Anyway, the false positive signal can be suppressed if formamide is added to the hybridization solution. Above ∼40% formamide, the three-base pair mutant is never observed and SNP detection becomes unambiguous. In optimal conditions, SNP detection gives a true-to-false signal ratio of 12 and compares favorably with allele-specific hybridization using dyes where the ratio is between 1 and 5.[34,35] The concentrations of formamide and NaCl to get such a ratio vary for different experiments, but the important parameter is their relative ratio. We work with concentrated salt solutions (1 M NaCl), and we pipet ∼1 μL of NaCl in an overall 50-μL incubation volume, which might lead to pipetting errors. In general, however, SNP detection with true-to-false ratios of >10 appear for formamide contents of 50−70% and NaCl concentrations of 25−40 mM. The conditions to reach SNP detection with nanocrystals are similar albeit more stringent than those used with dyes.

Other striking aspects of our DNA−nanocrystal conjugates are their stability, their fast hybridization, and their room-temperature incubation. DNA−nanocrystal conjugates stored at 4 °C maintain stable activity for more than 6 months. Also, the hybridization is carried out at room temperature; thus, no heating is necessary for the hybridization. We typically incubate the solution for 1 h to get SNP detection, but we found that incubation times of 10 min also yield a SNP detection signal with true-to-false ratios of >10. Such short incubation time was already noticed with CdSe/ZnS nanocrystals encapsulated into phospholipids micelles and modified by DNA.[12] Incubation times longer than 1 h did not result in higher signals.

The sensitivity of the nanocrystals does not reach that of the dyes yet, and this constitutes the weakest point of this technology for their use in DNA microarrays so far. There are essentially two reasons for this lower sensitivity. First, the single-wavelength laser diodes and the Axon scanner optics are optimized for Cy3 and Cy5 dyes. In this study, nanocrystals are excited at 532 nm where their cross section is relatively modest (Figure 1). Second, the density of the nanocrystals on the array may well be 1 order of magnitude lower than that of the dyes, as was observed in the case of DNA−gold conjugates.[3,36] Despite the lower sensitivity of our nanocrystals with respect to dyes in this study, simple modifications in the optical setup could greatly enhance the present sensitivity. For instance, nanocrystals have a continuous excitation band and an absorption cross section in the UV substantially higher than in the visible. A cross section 2 times higher results in a ∼10-fold increase in the number of photons absorbed. Thus, UV excitations would produce higher absorption and consequently higher fluorescence emission. Such sources include commercially available blue laser diodes with a 408-nm excitation line, Ar^+ lasers, and mercury or xenon lamps. On the other hand, the use of a grated spectrometer with CCD camera allows the unambiguous detection of at least four orthogonal channels in the visible range.[6,26] With such a setup, it has long been observed that nanocrystals photobleach at a much lower rate than organic dyes and that they can be detected at the single-molecule level for extended periods of time. Finally, commercially available quantum dots[15] have larger quantum yields than our samples and may further increase the overall sensitivity of this labeling technology. As a consequence, DNA−nanocrystals will be superior probes at spot sizes where the detection of dyes is limited by photobleaching. We view nanometer-size arrays as a potential technology where nanocrystals can surpass dyes. A DNA spot of ∼50 nm in diameter may contain only 100 probes. At this scale, the unambiguous detection of dyes with different colors is challenging, while it has become routine to detect multicolor single nanocrystals by stage-scanning confocal microscopy. [37,38]

Overall, our experiments indicate that DNA−nanocrystal conjugates have realistic potential for DNA microarray applications, for both SNP detection and multimarker detection. The stability and room-temperature hybridization condition make a nanocrystal/microarray-based field test a possibility. So far, our model system has used only synthetic targets, but we believe we can extend our results to real samples such as blood after appropriate extraction and purification of the genetic material. For instance, one application that can be derived from this study is to use nanocrystals and microarrays to do fast and full-panel viral and bacterial pathogen screening for blood banks. The microarray panel can include probes for hundreds of blood-borne pathogens such as hepatitis B virus, hepatitis A, C, D, E, F, G viruses, HIV, and sepsis-inducing bacteria. Another application is to use the SNP detection capability of nanocrystal−DNA conjugates to detect SNP arrays for different genes, such as the p53 oncogene in this study. Because of the superior true-to-false signal ratio and faster hybridization of the nanocrystal−DNA conjugates over other conventional labeling methods such as cyanine dyes, better discrimination and faster throughput can be achieved.

ACKNOWLEDGMENT

We thank Xavier Michalet for comments on the manuscript. This work was supported by NIH National Center for Research Resources through the University of California, Los Angeles subaward agreement 0980GCD709 through the U.S. Department of Energy under Contract DE-AC03-76SF00098, by NIH Grant 1R21CA95393-01, and by Basic Energy Sciences, Department of Energy.

Received for review May 7, 2003. Accepted July 3, 2003.

AC034482J

(34) Yang, Z.; Wong, G. K.; Eberle, M. A.; Kibukawa, M.; Passey, D. A.; Hughes, W. R.; Kruglyak, L.; Yu, J. *Nat. Genet.* **2000**, *26*, 13−14.
(35) Kwok, P. Y. *Pharmacogenomics* **2000**, *1*, 95−100.
(36) Willner, I.; Patolsky, F.; Wasserman, J. *Angew. Chem., Int. Ed.* **2001**, *40*, 1861−1864.
(37) Michalet, X.; Bensimon, A. *M. S.−Med. Sci.* **1997**, *13*, 1299−1305.
(38) Michalet, X.; Pinaud, F.; Lacoste, T. D.; Dahan, M.; Bruchez, M. P.; Alivisatos, A. P.; Weiss, S. *Single Mol.* **2001**, *2*, 261−276.